Selectivity and competition between the anodic evolution of oxygen and chlorine

Vos, J.G.

4

COMPETITION AND INTERHALOGEN FORMATION DURING PARALLEL ELECTROCATALYTIC OXIDATION OF BROMIDE AND CHLORIDE ON PT

Hydrogen production from seawater electrolysis is highly promising for the capture and storage of intermittent renewable energy. However, it is hindered by possible oxidation reactions of chloride and (to a lesser extent) bromide, which can occur in parallel to the evolution of oxygen and form harmful by-products. In this and the following chapter, we look deeper into these two unwanted side-reactions. First, we present general considerations of solution chemistry and oxidation products that may be expected in an acidic Br^-/Cl^- electrolyte. We then perform model studies of the parallel oxidation of Br^- and Cl^- and their mutual interaction on a Pt electrocatalyst, to increase the understanding of the anodic competition problem. Our results suggest that the oxidation of bromide is hindered by competing chloride adsorption on Pt, in a way that can be modelled quite well by a simple Langmuir isotherm describing the adsorption and reactivity of all species. The oxidation of chloride was however not properly captured by this same model. Furthermore, the formation of the interhalogen compound BrCl seems to occur in-between the oxidation of bromide and chloride.

THIS CHAPTER IS BASED ON THE FOLLOWING

PUBLICATION:

Vos, J. G.; Venugopal, A.; Smith, W.A.; Koper, M. T. M. Competition and Interhalogen Formation During Parallel Electrocatalytic Oxidation of Bromide and Chloride on Pt. Submitted to the Journal of the Electrochemical Society, under review (2019).

4.1. Introduction

As mentioned in section 1.2, seawater would be an extremely attractive substrate for solar energy conversion. Unfortunately, attempting to directly electrolyze a chloride-containing electrolyte may lead to the formation of large amounts of toxic chlorine on the anode. In addition to Cl^-, seawater contains a small but significant amount of Br^-, roughly 0.3mol% relative to chloride.[186] Analogous to the CER, bromide can rapidly be oxidized on the anode via the bromine evolution reaction (BER):

$$2\ Br^- \rightarrow Br_2 + 2\ e^- \qquad \text{Eq. 4.1}$$

$$E^0_{Br_2/Br^-} = 1.087\ \text{V vs. NHE}$$

Like chlorine, Br_2 is corrosive and toxic, and not easily disposed of in an environmentally friendly way. Its formation is unwanted but kinetically highly favorable during seawater electrolysis, due to the relatively low equilibrium potential relative to the OER. Bromide oxidation is also an especially important consideration during the electrochemical treatment and disinfection of wastewater, because it is strongly linked to bromination of organic waste compounds present in the water. This is highly detrimental to the detoxification performance.[187–189] The BER also is relevant to the energy intensive chlor-alkali process, where Br^- is a common contaminant in the brine feedstock.[190]

Previous literature has devoted far more attention to the CER than to the BER, in light of the former's industrial importance (see section 1.2). There has recently been a moderate increase in interest in the BER as it may be a useful reaction in redox flow batteries.[191,192] Much less research has gone into systems where both Cl^- and Br^- are present, such as when using seawater or a seawater-derived electrolyte, in which the BER and CER can occur simultaneously. To the best of our knowledge, the literature on this rather complex situation is scarce, and is mostly carried out from the perspective of wastewater treatment.[193–195] Our interest goes out specifically to the fundamental understanding of the parallel halogen oxidation reactions, which can be beneficial to seawater electrolysis and water treatment alike. The BER and CER seem to follow similar electrocatalytic pathways,[118,196–198] which implies that the active sites involved in the reactions would be the same, and that some form of interaction between them can be expected. One could then imagine that the two reactions simply mutually inhibit each other, or form an intimate coupling that can lead to changes in the reaction pathway and the formation of interhalogen compounds. Either case can have important practical implications, since in the first case, one reaction may block the occurrence of the other one if the ratio between reactants is unbalanced enough. In the latter, interaction between the two reactants can lead to unexpected outcomes.

In this chapter, we explore the parallel oxidation of bromide and chloride on a Pt electrocatalyst, which exhibits significant electrocatalytic activity for both the CER and BER. As a simplified model system, we use solutions containing HCl and HBr in varying ratios with additional $HClO_4$ as background electrolyte. This prevents the presence of cations in solution, which may have an influence on the kinetics.[96,199,200] The low pH was intended to prevent

complications from the formation of oxygenated chlorine or bromine species (such as ClO^- or BrO_3^-), which is favored by high pH,[201,202] and also allowed to study both the BER and CER on Pt with minimal interference from the OER. We utilize forced convection studies using an RRDE to gain insight into the kinetic competition and interdependence of the two reactions, coupled to a Pt ring that allows quantitative detection of soluble halogen products, similar to the discussion in Chapter 2. Special focus was on Tafel behavior and reaction orders as a function of potential and reactant concentration. Of special interest were mutual inhibiting effects, and the possible electrochemical formation of interhalogen compounds, such as BrCl. Kinetic studies were complemented with in-situ electrochemical UV-Vis experiments on stationary electrodes, to probe the formation of products as a function of potential and time near the electrode surface. The combination of these techniques sheds light on how chloride and bromide interact on a model electrocatalyst, and the implications this may have in a practical setting.

4.2. Experimental

All experiments were carried out at room temperature (~20 °C). Cleanliness protocols for the RRDE experiments were considerably more rigorous than those for the UV-Vis experiments, because forced-convection techniques are inherently more sensitive to contamination.

4.2.1. Chemicals

For the RRDE experiments, $HClO_4$ (70%, Suprapur®/Trace analysis grade) and HCl (30%, Ultrapur®/Trace analysis grade) were purchased from Merck. HBr (47%, Normapur®/Analysis grade) was purchased from VWR Chemicals. For the UV-Vis experiments, $HClO_4$ (60%, EMSURE/Analysis grade), HCl (32%, EMSURE/Analysis grade) and HBr (47%, EMSURE/Analysis grade) were purchased from Merck. All purchased chemicals were used as received. The water used for all experiments was prepared by a Merck Millipore Milli-Q system (resistivity 18.2 MΩcm, TOC < 5 p.p.b.).

4.2.2. Cleaning procedures

For the RRDE experiments, all glassware was thoroughly cleaned before first-time use by boiling in a 3:1 mixture of concentrated H_2SO_4 and HNO_3. When not in use, all glassware was stored in a 0.5 M H_2SO_4 solution containing 1 g/L $KMnO_4$. Before each RRDE experiment, glassware was thoroughly rinsed with water, and then submerged in a dilute (~0.01 M) solution of H_2SO_4 and H_2O_2 to remove all traces of $KMnO_4$ and MnO_2. The glassware was then rinsed three times with water and boiled in water. The rinsing-boiling procedure was repeated two more times.

The glassware and custom-built cell for UV-Vis experiments were cleaned by soaking in warm reagent grade 98% H_2SO_4 for an hour, followed by copious rinsing with Milli-Q water and boiling three times in Milli-Q water. When not in use, they were stored submerged in Milli-Q water.

4.2.3. Electrode preparation

4.2.3.1. RRDE experiments

Pt disks of 5 mm diameter (0.196 cm^2 geometrical surface area) were used as primary working electrode, along with a Pt ring as secondary electrode. At the beginning of an experimental session, the assembled Pt-Pt tip was rinsed with copious amounts of Milli-Q water, treated for 3 minutes with a solution of 0.5 M H_2SO_4 containing 0.5 g/L $KMnO_4$, rinsed with Milli-Q water, treated with a dilute (~0.01 M) solution of H_2SO_4 and H_2O_2 to remove any traces of $KMnO_4$ and MnO_2, and then extensively rinsed with warm (~50 °C) Milli-Q water. During RRDE experiments, the Pt disk and ring electrodes were electropolished by scanning from -0.1 V to 1.7 V at 500 mV s^{-1} for 20 scans at 1500 RPM. In-between experiments, the disk electrode was kept at 0.7 V vs. RHE. Ring currents were corrected for constant background currents and product collection delay. The latter arises from the time needed for products formed on the disk to reach the ring. The delay for each used rotation rate was empirically determined by stepping the potential to evolve Br_2 on the disk, and investigating the ring response as a function of time.

Before each experiment, the Pt electrode was subjected to a pre-treatment step to ensure an oxide-free, reproducible surface. The electrode was first kept at 0.4 V vs. RHE for 10 s, to reduce any residual trace of platinum oxide of preceding experiments, followed by a 3 s hold at 0.7 V vs RHE, to equilibrate the electrode and allow capacitive double layer charging to minimize. Scanning commenced immediately afterwards (see Figure A 9.3.1).

4.2.3.2. UV-Vis experiments

A 5 nm platinum layer was sputtered onto a conductive fluorine doped tin oxide (FTO) substrate (TEC-15, Hartford glass co.) for the in-situ UV-Vis transmission measurements. The deposition was performed at 3 µbar deposition pressure, with a deposition rate of ~0.593 Å/s, using an AJA sputtering system (ATC 2400). The FTO substrate was cleaned, prior to the deposition, using a sequence of laboratory soap, Milli-Q water, acetone and isopropanol and eventually drying the substrates with nitrogen gas. Subsequently, the FTO substrate surface was treated using argon plasma for 2 minutes, prior to the platinum layer deposition.

4.2.4. Cell preparation

4.2.4.1. RRDE experiments

RRDE experiments were done with home-made two-compartment borosilicate glass cells with solution volumes of 100 mL. An IviumStat potentiostat (Ivium Technologies) run by the IviumSoft software package was used for potential control. All experiments were done with an MSR rotator and E6 ChangeDisk RRDE tips in a PEEK shroud (Pine Research). All experiments were 95% iR-compensated during the experiment, by measuring the solution resistance with electrochemical impedance spectroscopy at 0.70 V vs. RHE, and observing the absolute impedance in the high frequency domain (100-50 KHz) corresponding to a zero-

degree phase angle. All solutions used were saturated with Ar (Linde, purity 6.0) before experiments. During forced convection experiments, solutions were continuously bubbled with Ar gas. The reference electrode was a HydroFlex® reversible hydrogen electrode (Gaskatel), separated from the main solution using a Luggin capillary. An additional LowProfile Ag/AgCl reference electrode (Pine Research) served to measure the solution pH and was used for conversion to the NHE scale. The Ag/AgCl reference was externally calibrated on a regular basis and had a value of 198 ± 0.5 mV vs. NHE. All potentials in this chapter are reported on the NHE scale unless explicitly mentioned otherwise. A flame-annealed Pt mesh was used as counter electrode, separated from the main solution by a coarse sintered glass frit.

4.2.4.2. UV-Vis experiments

A Vertex potentiostat (Ivium Technologies) run by the IviumSoft software package was used for potential control. The transmission measurements were performed in a custom-built setup, consisting of a PTFE electrochemical cell housing equipped with quartz windows. A coiled platinum wire acted as the counter electrode, and a LowProfile Ag/AgCl reference electrode (Pine Research) was placed in fixed position relative to the Pt/FTO working electrode. The Ag/AgCl electrode was calibrated at 199 ± 0.5 mV vs. NHE. All applied potentials were 90% iR-compensated according to the solution resistance. The latter was measured using a similar procedure as in the RRDE experiments (section 4.2.4.1). A combination of light sources, a deuterium lamp (Mikropack D-2000) and a halogen lamp (Ocean Optics HL 2000 – FHSA), were used in the setup. These sources were combined using an optical fiber arrangement and this fiber acted as the illumination source for the transmission measurements. The setup also included a spectrometer (Ocean Optics, Maya 2000 Pro), which was used to capture the transmitted light. The setup was aligned in such a way that the platinum/FTO sample was illuminated from the back side and the transmitted light was captured on the opposite side of the electrochemical cell. The transmission data was continuously recorded in-situ, while performing the electrochemical measurements.

4.3. Results and discussion

4.3.1. Brief review of the BER and CER kinetics on Pt

The experimental CER kinetics on Pt appear the most compatible with the Volmer-Tafel (V-T) mechanism, as suggested by Conway and co-workers. Evidence comes from impedance studies,[108] potential-relaxation experiments[203] and recombination test plots,[204] showing that Eq. 1.19 gives a good fit of the experimental data. However, the interpretation of experimental reaction orders has been much less straightforward. This may be in large part due to the complicating effect of transient formation of platinum oxide (PtO_x), which readily occurs at potentials where the CER takes place (section 4.3.5). The oxide layer competes with Cl^- adsorption during CER electrocatalysis, and may itself have an effect on intrinsic catalytic rates.[56,205] Conway and Novák obtained chloride reaction order values close to 1 when $[Cl^-]$ = 100 mM, decreasing to zero when $[Cl^-]$ increased to 1 M and higher.[118] These values were

measured at constant overpotential, for which the V-T mechanism predicts that $\mathcal{R}_{Cl^-} = 0$ (see section 9.4.3). The authors explained the non-zero values by the effect of specifically adsorbed chloride anion (Cl^{-*}) on the PtO_x layer, but no further analysis was undertaken to explore this. The BER mechanism on Pt has been much less studied,[206–208] but previous work by Conway *et al*. with similar methodology as used for the CER indicates that it follows V-T characteristics when $[Br^-] > 1$ M.[196] The bromide reaction order was however not investigated in their work. The effect of oxides during the BER should be much lower, because the BER takes place at lower potentials than the CER. Additionally, bromide has a much stronger oxide suppressing effect compared to chloride. In a mixed Br^- + Cl^- electrolyte, the situation becomes more complex, since multiple electroactive species are involved with differing adsorption strengths.[209] We will focus our study on mutual competitive blocking effects, since these should be relevant to the catalytic activity in an actual electrolyzer. Additionally, co-adsorption of the two halogens could lead to the evolution of interhalogen compounds, such as BrCl. We will show below that this compound may indeed be electrochemically formed. We assume that the direct electrochemical formation of triatomic interhalogen ions through a trimolecular reaction, such as $BrCl_2^-$, is highly improbable.

4.3.2. Considerations of interhalogen formation reactions

When carrying out electrolysis in a mixture of halogen anions, one needs to consider various electrode reactions and solution reactions, as summarized in Scheme 1. The corresponding equilibrium constants of these reactions are given in Table A 9.4.1.[202,210]

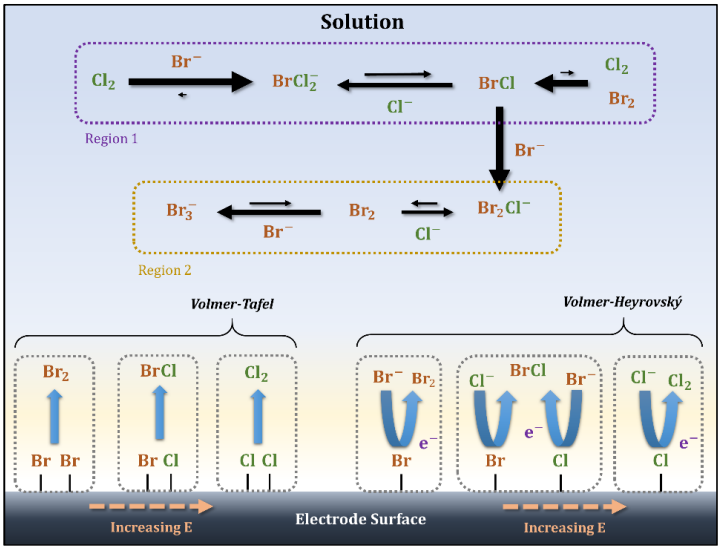

Scheme 4.1: Halogen reaction pathways on Pt during the parallel oxidation of aqueous Br^- and Cl^- in an acidic solution, according to data from literature[210] and Table A 9.4.1. Black arrows represent solution phase reactions, relative sizes and thicknesses between pairs are illustrative of the direction of the corresponding equilibrium. Blue arrows represent elementary steps in electrochemical reactions on the electrode surface. Bottom area left shows rate-limiting reaction steps according to the Volmer-Tafel mechanism, which most likely dominates on Pt. The right shows rate-limiting reaction steps according to a Volmer-Heyrovský or Volmer-Krishtalik-type mechanism. We exclude trimolecular reactions in this scheme.

In Scheme 4.1, solution phase reactions are drawn starting from Cl_2 and ending in Br_3^- as the most stable species. Two 'regions' can be discerned in the overall pathway: one that comprises the interconversion between stronger oxidizing species Cl_2, $BrCl_2^-$ and BrCl, and region 2 consisting of Br_2, Br_2Cl^-, and Br_3^-, species with higher stability. Besides effects of kinetic competition, we are interested if electrocatalytic interhalogen formation can occur in a mixture of Br^- and Cl^-. As discussed in section 4.3.1, the main reaction of interest is the formation of BrCl according to:

$$Br^- + Cl^- \rightleftharpoons BrCl + 2\,e^- \qquad \text{Eq. 4.2}$$

This previously unreported reaction falls thermodynamically in-between the BER and the CER (see Table A 9.4.1). It is illustrated in the lower part of Scheme 4.1, along with the BER and CER, displaying the Tafel reaction (bottom left) or electrochemical desorption (bottom right) as the rate-limiting step.

Unfortunately, accurate determination of products formed electrochemically on the electrode is not straightforward in this system, because the aqueous interhalogen reactions shown in Scheme 4.1 and Table A 9.4.1 are extremely rapid (values of rate constants are typically in the order of 10^9). Any 'oxidizing equivalents' (thermodynamically labile species) generated on the electrode will therefore tend to dissipate by reacting with bulk surplus of Br^- and Cl^- in solution, which obfuscates the identity of the electrochemical product originally formed.[211] Given sufficient mixing, the system will always evolve towards a mixture of primarily Br_2, Br_3^- and Br_2Cl^-, regardless of the electrode potential applied. Although we thus cannot pinpoint exactly the origin of any halogen species near the electrode, we can still rationalize the occurrence of reactions happening in-between the BER and the CER from thermodynamic constraints. Equilibrium constants in Table A 9.4.1 show large differences in the stability of several species. In case that only Br_2 is being generated at the electrode, this implies that no interhalogen other than Br_2Cl^- should be formed spontaneously in solution, as the driving force for the other interhalogen species is too small. The occurrence of either BrCl or $BrCl_2^-$ at electrode potentials lower than the thermodynamic onset of Cl_2 evolution can then only be rationalized by the occurrence of an electrochemical reaction. When the potential is high enough to allow Cl_2 evolution, all species Scheme 4.1 can in principle be formed. The most interesting potential region is thus in-between the BER and CER.

4.3.3. RRDE studies of parallel oxidation of bromide and chloride

We used RRDE voltammetry to study the kinetics of parallel oxidation of Br^- and Cl^- under hydrodynamic conditions, as this greatly simplifies the analysis by keeping the diffusion layer thickness constant. It also removes products from the surface that may possibly react further and in this way influence the apparent electrochemical kinetics;[208] this could be either follow-up electrochemical reactions on the surface, such as the oxidation of Br_2 into BrO_3^-, or through interhalogen reactions in the solution (see section 4.3.2). The RRDE also allows following the formation of soluble reaction products by utilizing a Pt ring as detector. The ring potential was fixed at 0.7 V vs. RHE, to reduce halogen species formed on the disk without also reducing O_2.

Although the onset for oxygen reduction is around 0.95 V vs. RHE on Pt in $HClO_4$, the adsorption of Br^- significantly increases the overpotential, reducing oxygen reduction to negligible rates for potential values down to 0.7 V vs. RHE.[212] It was found that Br_2 reduction becomes diffusion limited at an overpotential of approximately $\eta \approx 150$ mV (see Figure A 9.4.1 for details). Additionally, in Chapter 2 we showed that Cl_2 reduction on Pt becomes diffusion limited at $\eta \approx 250$ mV. Ring currents at 0.7 V vs. RHE can thus be taken as quantitative.

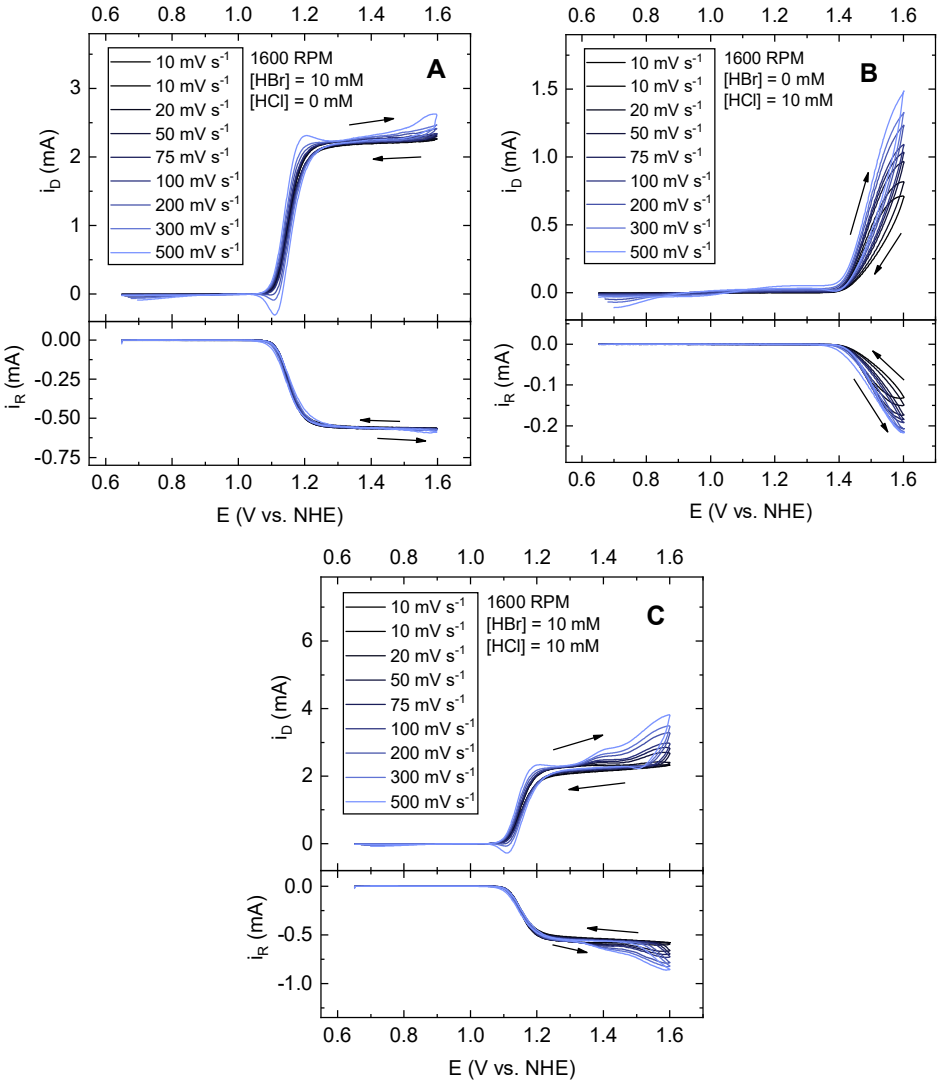

Figure 4.1: Cyclic voltammograms of a Pt-Pt RRDE in a solution of 0.1 M $HClO_4$, showing the BER in presence of 10 mM HBr (Panel A), the CER in presence of 10 mM HCl (Panel B), and parallel oxidation of Br^- and Cl^- in presence of 10 mM HBr + 10 mM HCl (Panel C). Varying scan rates are shown in shades of blue at a fixed rotation rate of 1600 RPM. Top panels show disk currents, bottom panels show ring currents while keeping the ring potential at 0.7 V. Arrows indicate scan direction.

Throughout this chapter we generally use the NHE as potential scale. We note that the pH-dependent formation of platinum oxide (PtO_x) can have a large effect on the apparent reaction kinetics.[58,203,205] A change in acid concentration can thus cause a shift in the potential of oxidation of the Pt surface on the NHE scale, and correspondingly the catalytic activity. The significant background acid concentration of 0.1 M $HClO_4$ served to dampen pH changes as the total acid concentration was changed. The highest observed pH change was around 0.3 pH unit, when going from 100 mM $HClO_4$ to 100 mM $HClO_4$ + 10 mM HBr + 100 mM HCl, which is equivalent to a potential difference of about 20 mV.

Figure 4.1 shows the BER and CER (panels A and B) as well as parallel Br^- and Cl^- oxidation (panel C) on a Pt-Pt RRDE, for varying scan rates. In Figure 4.1A, the BER starts at a potential of 1.05 V, corresponding to a negligible overpotential, and reaches a plateau current at approximately 1.25 V. In control experiments using 5 mM HBr (not shown), the measured values of the BER limiting current correspond within a few % to a previous report by Xu *et al.*[208] The value is approximately 90% of the theoretical value predicted by the Levich equation, suggesting that the limitation stems from mass transport and that it is not due to kinetic limitations which may occur at much higher bromide concentrations.[196] The effect of scan rate on the BER is minimal for slow to modest scan rates up to 75 mV s^{-1}. At higher rates, the inability of Br_2 to be transported away from the surface fast enough leads to additional reactions. The oxidation of Br_2 to BrO_3^- is visible around 1.50 V in the forward scan,[213] and the reduction of Br_2 to Br^- in the backward scan near 1.10 V. The CER in Figure 4.1B starts at 1.37 V, which like the BER is very close to its thermodynamic value. Contrary to the BER, it has a rather strong scan rate dependence. This effect can be explained by transient oxidation of the

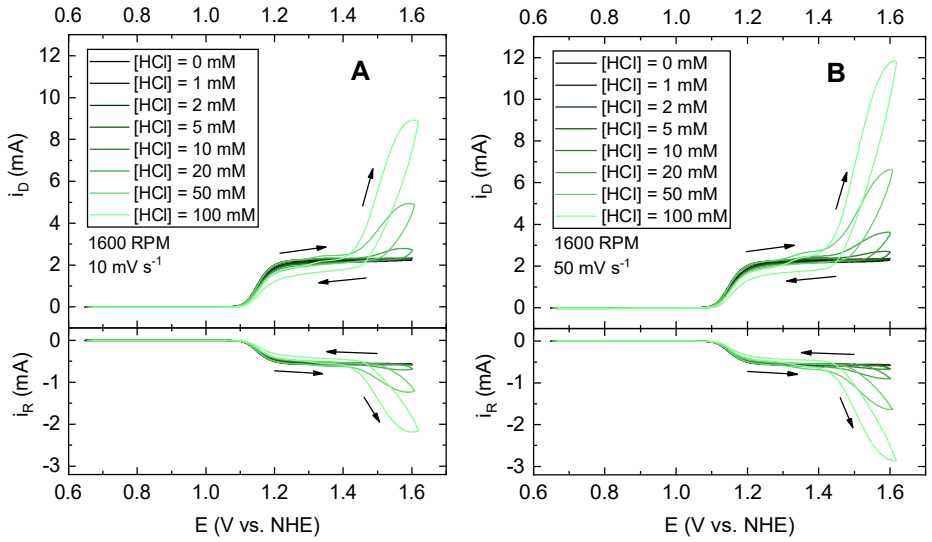

Figure 4.2: Cyclic voltammograms of a Pt-Pt RRDE in a solution of 0.1 M $HClO_4$ + 10 mM HBr, showing the effect of varying HCl concentrations in shades of green, recorded at 10 mV s^{-1} (A) and 50 mV s^{-1} (B) at a fixed rotation rate of 1600 RPM. Top and bottom panels like those described in Figure 4.1. Arrows indicate scan direction.

Pt surface. PtO_x has very poor catalytic activity for the CER, and its formation is a relatively slow process on the timescale of this experiment.[108,196] A faster scan rate then leads to a Pt surface that is less oxidized when CER becomes thermodynamically favorable, and thereby results in higher reaction rates. This will be discussed in more detail below. In Figure 4.1C, the presence of both 10 mM HBr and 10 mM HCl leads to the same current plateau as seen in the BER wave in Figure 4.1A, followed by two superimposed current waves, a first with an onset around 1.30 V, and a second one with an onset potential of 1.42 V. The latter one should correspond to CER. The wave starting at 1.30 V must correspond to the interaction between bromide and chloride. We will analyze the competition between BER and CER and their interaction in more detail in the subsequent sections.

Figure 4.2 shows parallel Br^- and Cl^- oxidation with varying HCl concentration, for two different scan rates. The superimposed oxidation wave between 1.30 – 1.65 V is chloride concentration dependent, including the 'pre-peak' that starts around 1.30 V. They experience an increase in current and lowering of the onset potential with increasing Cl^- concentration. The pre-peak is also clearly captured in the ring currents (Figure 4.2 bottom panels), so that it must correspond to a halogen evolution reaction. Diffusion-limited bromide oxidation (potential region of 1.20 – 1.30 V) seems rather unaffected by the increasing presence of chloride, except when $[Cl^-] = 100$ mM, where a kind of inhibition occurs.

The Pt ring electrode was used to quantify the extent to which the currents observed on the disk corresponded to the evolution of soluble product species (Figure 4.1 and Figure 4.2, bottom panels). The ring currents clearly mark the onset of the halogen oxidation reactions. Particularly in Figure 4.1C, the ring effectively mirrors the disk during halogen oxidation. Once halogen oxidation reactions start occurring, the ratio $|i_R/i_D|$ generally converges to a constant value that is within 2% of the RRDE collection factor (Figure A 9.4.3 and Figure A 9.4.4). Scan rates faster than 100 mV s^{-1} lead to some deviation from steady-state values, due to pseudocapacitive contributions on the disk (such as from PtO_x-related reactions), as well as a decrease in the time resolution of the ring response.[214] At high CER overpotentials in high Cl^- concentrations we also saw systematic deviations (Figure A 9.4.6), likely because the ring response became distorted by bubble formation during intense gas evolution on the disk (see also Chapter 8). In low Cl^- concentrations all scan rates show a slight decrease in ring/disk ratios above 1.55 V, likely due to the onset of slow parallel evolution of O_2 on the disk. The OER contribution on the disk is nonetheless rather small (less than 1%). In summary, all disk current can be ascribed to only halogen oxidation for any combination of [HCl], scan rate or rotation rate, as long as the scan rate does not exceed extreme values (see also Figure A 9.4.5).

4.3.4. Bromide oxidation and the effect of chloride

In this section, a closer look into the effect of chloride on the oxidation of bromide will be taken, primarily by investigating Tafel slopes, reaction orders and the effect of mass transport. Koutecký-Levich plots of the bromide oxidation wave at various chloride concentrations were constructed using the forward sweeps of CVs (See Figure A 9.4.10). The y-intercepts were then calculated as function of potential (Figure A 9.4.11). These results show that a higher $[Cl^-]$

causes an increasing degree of kinetic control over the reaction, although the effect is very subtle when $[Cl^-] < 100$ mM.

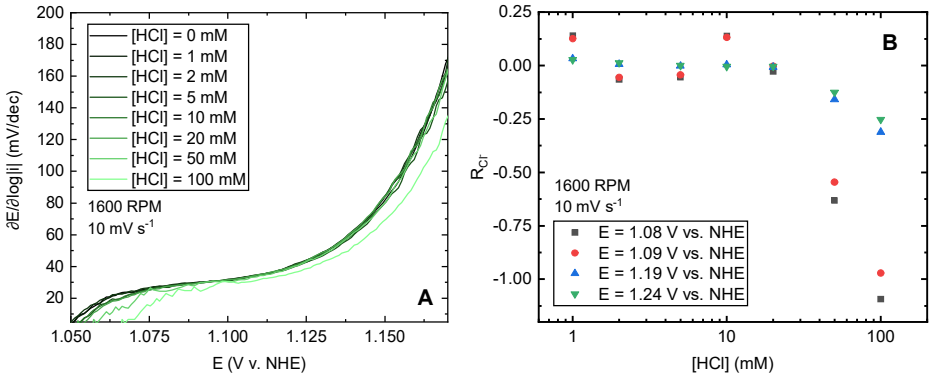

Figure 4.3: Tafel slope values in the bromide oxidation region of Figure 4.2A (A) for various measured chloride concentrations. Only forward scans are shown. B: Chloride reaction order $\mathcal{R}_{Cl^-}$ as function of chloride concentration, based on data shown in Figure A 9.4.9B.

Figure 4.3A shows Tafel slopes (derived from Figure A 9.4.8B) as a function of potential. From Figure A 9.4.11, we can discern the potential region of roughly 1.075 – 1.125 V as kinetically limited. In this region the Tafel slopes show a fairly constant value between 25-35 mV/dec, agreeing well with previously reported values.[196] Addition of chloride up to concentrations of 50 mM does not change the Tafel slope values, and chloride reaction order analysis (Figure 4.3B) shows that $\mathcal{R}_{Cl^-}$ stays close to 0. The effect of changes in PtO_x coverage due to varying pH should be very minor. Control experiments with 10 mM HBr and no chloride showed that the BER rates show no hysteresis up to 1.40 V, suggesting that inhibiting PtO_x, though it may be formed,[207] plays no significant role in the apparent catalytic activity (Figure A 9.4.12). The reaction becomes notably affected when the chloride concentration increases to 100 mM, where the Tafel slope values rise less quickly as function of potential, and $\mathcal{R}_{Cl^-}$ decreases to around -1.

We also measured the BER dependence on bromide, in absence and presence of an excess of chloride as to further probe the latter's competition behavior. Figure A 9.4.13 and Figure A 9.4.14 show bromide oxidation curves and derived Tafel slopes as function of $[Br^-]$. Tafel slope values of the BER in 1 M HCl (Figure A 9.4.14B) are overall higher (30-50 mV/dec) and significantly less linear, as would be expected on the basis of Langmuirian competitive adsorption (Section 1.2 of the SI). Figure A 9.4.15 displays $\mathcal{R}_{Br^-}$ for 10 mM $\leq [Br^-] \leq$ 100 mM. The values around each given $[Br^-]$ are shown versus potential, because the BER is too fast to measure activation controlled currents over a wider range of $[Br^-]$ at a fixed potential, without running into diffusion limitations. The quasi-linear regions in Figure A 9.4.14 were used to approximate the activation-controlled region for each $[Br^-]$. Experimental error from very small currents and the possible influence of the backward reaction led to unexpectedly high values of $\mathcal{R}_{Br^-}$ at very low overpotentials. Nonetheless, for each $[Br^-]$ in their respective activation controlled potential region, $\mathcal{R}_{Br^-}$ values are arguably close to 2, as predicted by the V-T mechanism. The apparent reaction orders rapidly approach 1 as the potential increases,

due to mass transport control. Interestingly, Ferro *et al.* obtained $\mathcal{R}_{\mathrm{Br}^-} \approx 1$ on a stationary Pt electrode;[213] these values were obtained at constant overpotential, but the value of E_{eq} was kept fixed by adding equimolar amounts of $\mathrm{Br}^- + \mathrm{Br}_2$, such that expected values of $\mathcal{R}_{\mathrm{Br}^-}$ are within 2 and 0. Considering the rather narrow (roughly 50 mV) potential ranges in Figure A 9.4.15 where the BER appears activation controlled, it is possible that their values were unintentionally obtained under diffusion controlled conditions.

When regarding the effect of competitive Cl^- adsorption, one can extend the bromide adsorption isotherm to include both Br^- and Cl^- according to:

$$\theta_{Br} = \frac{K_{Br}[\mathrm{Br}^-]e^{f\eta}}{K_{Br}[\mathrm{Br}^-]e^{f\eta} + K_{Cl}[\mathrm{Cl}^-]e^{f\eta} + 1} \qquad \text{Eq. 4.3}$$

A detailed discussion of the mechanistic implications of Eq. 4.3 can be found in section 9.4.2. Importantly, it leads to the same predictions for $\mathcal{R}_{\mathrm{Br}^-}$ as in absence of competition, namely that $\mathcal{R}_{\mathrm{Br}^-}$ should consistently decrease from 2 to 0 as a function of $[\mathrm{Br}^-]$ in the V-T mechanism. In presence of an excess of 1 M Cl^- in Figure A 9.4.15A, $\mathcal{R}_{\mathrm{Br}^-}$ has overall slightly lower values. The reaction is no longer fully diffusion-controlled such that $\mathcal{R}_{\mathrm{Br}^-}$ is no longer strictly 1 at higher potentials. The data seem to approach a non-zero value with higher potential, and again approach 2 at low overpotentials. Both observations are predicted by the V-T pathway under the assumption of Langmuirian, competitive adsorption. From this, we conclude that chloride acts as an inhibitor on bromide oxidation and is otherwise uninvolved. Because chloride typically binds weaker to surfaces than bromide,[215] we expect that only at high ratios of chloride versus bromide (such as in seawater), where $K_{Br}[\mathrm{Br}^-] \ll K_{Cl}[\mathrm{Cl}^-]$, the BER may become significantly slowed down.[216]

4.3.5. Chloride oxidation and the effect of bromide

In this section, we look more closely how the oxidation of chloride is affected in a mixed $\mathrm{Br}^- + \mathrm{Cl}^-$ electrolyte. The pre-peak starting at 1.30 V (Figure 4.1 and Figure 4.2) suggests a more complex Br and Cl interdependence than only competitive adsorption, which is most likely due to the formation of BrCl. The nature of this process will be discussed separately in section 4.3.6. For a meaningful analysis, it is necessary to isolate the chloride oxidation current from the superimposed BER current plateau. A strict separation is complicated, because the oxidation pathways of Br^- and Cl^- are clearly mutually dependent and the underlying contribution of each pathway is not exactly known. As a first approximation, we assumed that the BER follows an ideal sigmoidal curve, which appears justified by results from section 4.3.4 and Figure A 9.4.12. The BER wave could then be fitted using a 5-parameter generalized logistic function, whose relative complexity allowed modelling the asymmetry that is inherent to reaction mechanisms more complex than a single electron transfer step.[217] The procedure is illustrated in Figure A 9.4.23.

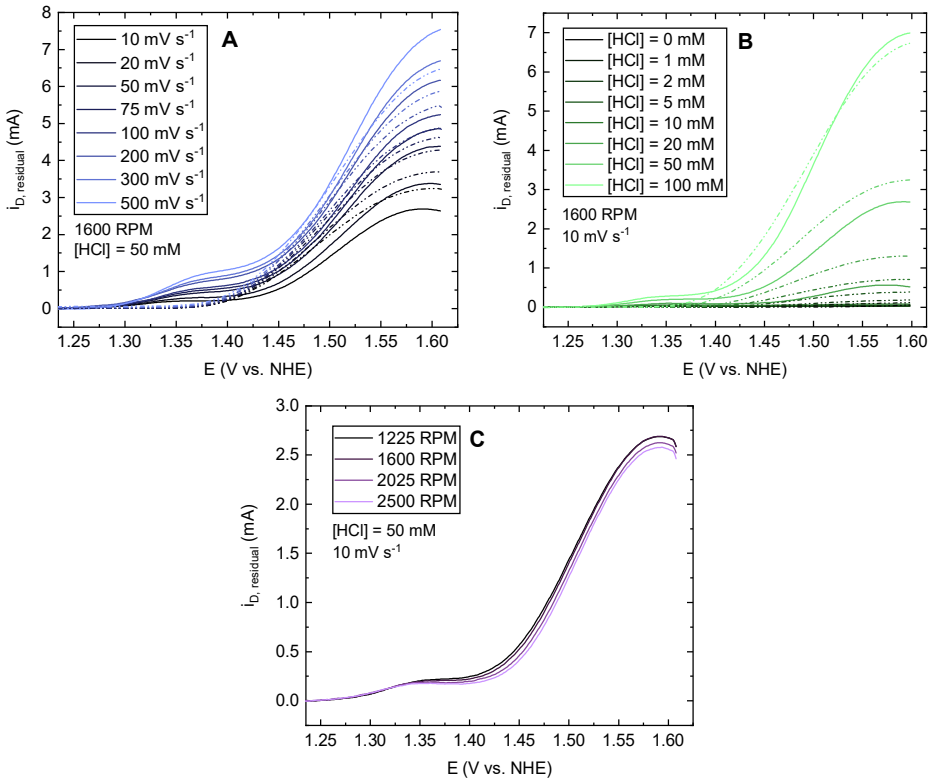

Figure 4.4: Residual chloride oxidation currents after subtraction of BER-related current using a generalized logistic baseline. Shown are the effect of scan rate (A), HCl concentration (B), and rotation rate (C). Dashed lines in A and B correspond to CER data measured in absence of Br^- under otherwise identical conditions.

Figure 4.4 shows the effect of various experimental parameters on the current related to chloride oxidation, after applying a logistic baseline correction for the superimposed BER current. In comparison with the dashed traces of 'pure CER current' under bromide-free conditions, there are significant differences. The 'main' oxidation wave, with an onset of 1.45 V in Figure 4.4A, can be ascribed to the CER. The overpotential for the CER in Figure 4.4A and B is generally increased relative to bromide-free conditions, except for the experiments with the highest scan rates and chloride concentrations. Figure 4.4C furthermore shows that the CER current slightly decreases with rotation rate. This behavior may be caused by an increase of the steady-state bromide coverage θ_{Br} as a result of increased mass transport, leading to suppression of the CER. When $[Cl^-]$ was increased to 100 mM such that the BER became more inhibited (section 4.3.4), the CER displayed an increase in current with rotation rate, but a more clear rotation rate dependence could not be established (Figure A 9.4.16).

The CER is much more likely to be affected by PtO_x formation, for which the driving force is significant near the CER equilibrium potential. Oxide growth causes the CER current in Figure 4.4 to level off or sometimes even decrease with higher potential. The highest recorded currents in Figure 4.4B are less than 10% of the diffusion limitation predicted by the Levich equation, showing that the reactivity limitation is a kinetic effect.

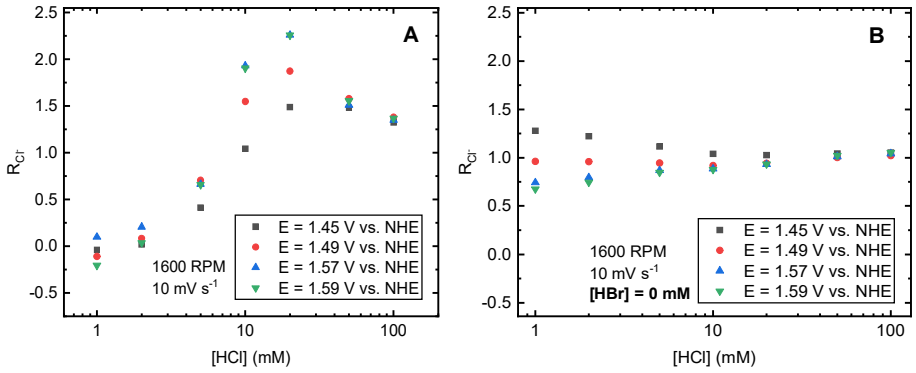

Figure 4.5: Chloride reaction order $\mathcal{R}_{Cl^-}$ as function of chloride concentration, based on data from Figure 4.4B. Shown are values in presence of 10 mM HBr (A), as well as those in bromide-free conditions (B).

Figure 4.5 shows chloride reaction orders based on data from Figure 4.4B. In presence of Br^- (Figure 4.5A) the reaction order is close to 0 at low chloride concentration, but then increases to values close to 2, and then assumes a value of ~1.4 at $[Cl^-] = 100$ mM. This is in remarkable contrast to the results obtained in absence of Br^- (Figure 4.5B), for which reaction orders are close to 1, regardless of potential or chloride concentration.

All results in Figure 4.5 should contain a contribution from transient formation of the PtO_x layer. For the CER, this 'oxide reaction order' has been studied previously by Conway and Novák, who obtained steady $\mathcal{R}_{Cl^-}$ values between 0.8 - 0.9 which quite suddenly decreased to 0 as $[Cl^-]$ increased to 1 M, at constant overpotential (see also section 4.3.1). As mentioned previously, the V-T mechanism predicts that $\mathcal{R}_{Cl^-}$ is always zero when considered at constant overpotential. The contradicting non-zero values were ascribed to specific adsorption by Cl^- at the expense of the oxide layer, forming co-adsorbed 'Cl^{-*}' which saturates to a constant value at higher concentrations. This explanation is however not completely sufficient, since the surface reaction order $\partial \ln \theta_{Cl} / \partial \ln[Cl^-]$ is then still expected to vary between 1 and 0, and thus the overall reaction order should again be $0 \leq \mathcal{R}_{Cl^-} \leq 2$. Most importantly, $\mathcal{R}_{Cl^-}$ should not be consistently near unity, but should vary as a function of $[Cl^-]$ and potential. The V-T mechanism predicts the same when measurements are made at constant potential, such as in our results in Figure 4.5B. Similar to Conway and Novák's results, they do not agree satisfactorily with the usual kinetic models.

Br^- is also known to inhibit the oxidation of platinum, and does so more strongly than Cl^-.[206,218] Br^- may thus affect the CER indirectly by replacing PtO_x as the competitive adsorbate, which could change the apparent reaction order values between Figure 4.5A and B. In order to look into this more closely, one could describe the effect of adsorption from either Br^- or PtO_x using a site-blocking model. Previous studies have shown that the oxide layer on Pt initially forms up to a monolayer of OH^*, and O^*, coupled to a slow place-exchange between O and Pt as oxidation progresses.[219,220] For a fixed potential E, this oxide growth depends on time according to:[205]

$$Q_{PtO_x}(t) = A(E)\log(t + t_0) \approx A(E)\log(t) \qquad \text{Eq. 4.4}$$

In this equation, Q_{PtO_x} is the charge transferred in the formation of the layer, which can be measured from the corresponding reduction peak, t_0 is a offset time present at the start of the linear $\log(t)$ region (usually, $t_0 \ll t$), and A is an empirical constant that depends on the potential. The oxide growth has been reported to depend on time as $\log(t)$ over a wide range of time and potential values, including when chloride is present in the electrolyte.[205] In our potentiodynamic experiments, the overall polarization time and thus the expected oxide thickness should then approximately depend on the scan rate ν for a given potential window and electrolyte composition according to:

$$Q_{PtO_x} \propto \log\left(\frac{1}{\nu}\right) \qquad \text{Eq. 4.5}$$

Values of Q_{PtO_x} were obtained from the PtO_x reduction peak (Figure A 9.4.17). As predicted by Eq. 4.5, a plot of Q_{PtO_x} vs. $\log(\nu)$ resulted in a straight line with negative slope in 0.1 M $HClO_4$. This relationship was preserved in presence of 10 mM Br^- (Figure A 9.4.18). It was also preserved in the combined presence of Br^- + Cl^-, suggesting that PtO_x shows the same growth characteristics under influence of the two halogen anions. When CER current values are then compared versus Q_{PtO_x}, a quite linear relationship emerges (Figure A 9.4.19 and Figure A 9.4.20). It can be reasonably assumed that sub-monolayers of oxide were present during most experiments, since in our case the charge of a 'monolayer' oxide on a perfectly flat surface corresponds to roughly 80 µC.[205] These results thus suggest that the effect of PtO_x on the CER activity is primarily through site-blocking. A similar observation underlies the work of Patil *et al.*[221] Further evidence comes from Figure A 9.4.23: Currents recorded at 1.57 V (Figure A 9.4.22) were extrapolated to $Q_{PtO_x} = 0$ (a 'PtO_x-free' surface), and were normalized to the chloride concentration. Comparison with diffusion-limited currents predicted by the Levich equation (blue) suggests that the CER would reach diffusion-limited currents in absence of oxides at 1.57 V. There may also be an intrinsic catalytic effect of the oxide layer, but this is likely most significant at specific oxide coverages that are close to (formally) a monolayer.[118,205]

Contrary to PtO_x, the adsorption of Br^- is in pseudo-equilibrium and should be regarded in the same way as the CER, such as by using the competitive Langmuir isotherm in Eq. 4.3. However, the results from Figure 4.5A strongly disagree with the prediction that $\mathcal{R}_{Cl^-}$ should consistently decrease from 2 to 0 as a function of $[Cl^-]$. Instead, $\mathcal{R}_{Cl^-}$ stays close to 0 for an appreciable concentration range and then increases. A simple Langmuirian site-blocking description therefore seems inadequate. The chloride reaction orders in Figure 4.5A also seem incompatible with a change in reaction pathway towards BrCl formation, since it is expected that $\mathcal{R}_{Cl^-} \leq 1$ for this reaction.

Figure 4.6 shows measured Tafel slope values for the CER in presence (A) and absence (B) of Br^-. 'Pure CER' in Figure 4.6B for various chloride concentrations has linear Tafel regions with a slope between 35-45 mV/dec, in agreement with previous results,[58] followed by a continuous increase in slope with higher potential. The latter is explained by (transient) inhibition of the CER due to PtO_x formation, as was previously noted. The effect lessens as the chloride concentration increases. Like in Figure 4.5, the presence of Br^- imparts significant

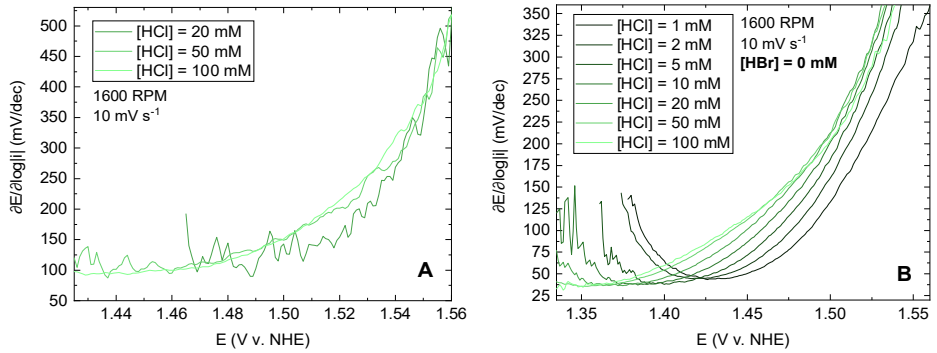

Figure 4.6: Tafel slope values in the CER region of Figure 4.4B following the pre-peak, for the various measured chloride concentrations. Only forward scans are shown. Shown are values in presence of Br^- (A), and values for 'pure CER' in absence of Br^- (B). Several traces in A and B involving 0-10 mM chloride have low signal/noise ratios and are not shown or have been cut off at lower potentials.

changes. Intriguingly, the linear Tafel regions now have a value of around 100 mV/dec. In the Langmuir isotherm, competition leads to higher Tafel slope values (see Table A 9.4.2), but only in combination with increasing curvature. It cannot explain Tafel regions that have a higher value, but also stay linear. The linear value of 100 mV/dec could imply that a change in the rate-determining step of the CER mechanism has taken place, the most straightforward possibility being rate-limiting Volmer discharge. This, however, is in contradiction with $\mathcal{R}_{Cl^-}$ being greater than 1 in Figure 4.5A. In summary, chlorine evolution seems to be the major reaction in the chloride oxidation region, but presence of Br^- induces a large change in the apparent kinetics. This change does not stem from a change in how the oxide layer forms during the experiments, but seems to be the result of a complex interaction of Br^- or Br^* with the CER reaction pathway on the surface. The CER on Pt, regardless of the presence of Br^-, is not captured by the usual microkinetic models in a fully satisfactory way, as was previously hinted at by Tilak and Conway.[112]

4.3.6. Nature of the chloride oxidation pre-peak

As mentioned above, the pre-peak that starts at 1.30 V only appears when both Br^- and Cl^- are both present, at a potential where the BER is diffusion limited, and where the CER is thermodynamically not yet allowed, meaning it cannot be ascribed to the evolution of either Br_2 or Cl_2. At the same time, the pre-peak current is always registered on the ring, so that it is associated with the evolution of a soluble reaction product. Therefore, it likely involves formation of an interhalogen compound, where BrCl is the most probable candidate, as its standard potential (1.19 V vs. NHE) lies in-between CER and BER.

To investigate the pre-peak in more detail, it was necessary to extend the fitting procedure discussed in section 4.3.5 to 'isolate' the relevant current. It must be noted that the pre-peak is always convoluted by parallel evolution of bromine and chlorine. The BER contribution was previously modelled using a generalized logistic function, such that the residual current contains the CER wave with the pre-peak superimposed. To isolate the pre-peak current, the CER wave was modelled using a simple exponential function according to the Butler-Volmer

relation. CER curves were fitted using narrow potential regions where the Tafel slope was roughly constant as in Figure 4.6. The resulting exponentials were then extrapolated under the pre-peak, forming a nonlinear baseline together with the generalized logistic function for the BER. The multistep nature of the reaction could justify a more complex fitting function, but as discussed in section 4.3.5, this relation need not hold at potentials higher than the linear Tafel regions, where the real kinetics are obscured by PtO_x formation. The entire procedure thus assumes that the BER and CER are the main reactions occurring in a mixed Br^- and Cl^- electrolyte, behaving respectively as an asymmetric sigmoid and (at low overpotentials) a superimposed exponential, and that the pre-peak is a third process overlapping with the previous two. In case that the CER currents were too small to observe a linear Tafel region, a simple linear baseline was used instead.

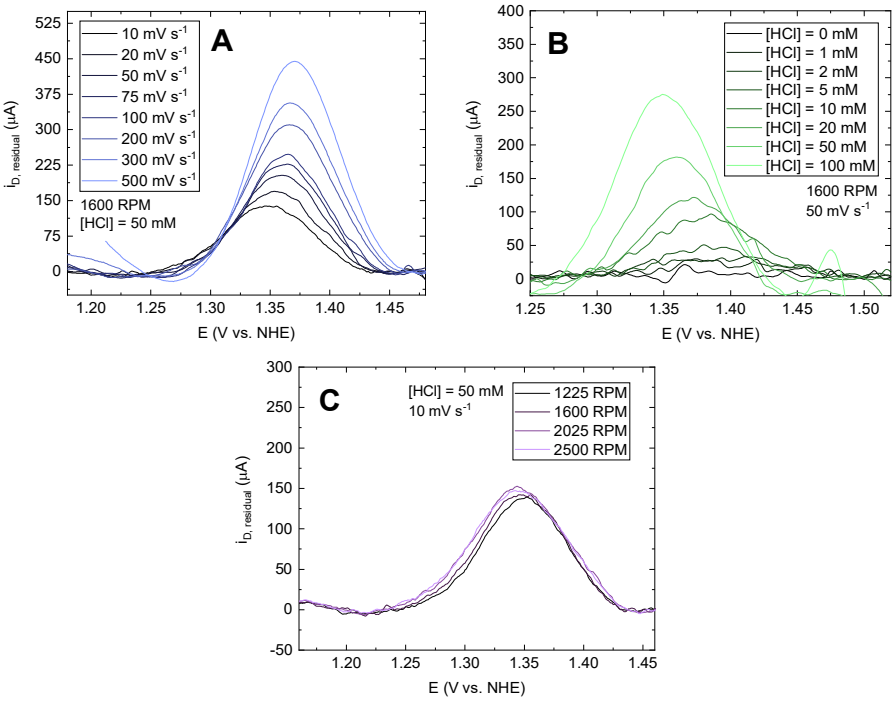

Figure 4.7: Examples of chloride oxidation pre-peak current determined from RRDE experiments, after separating BER and CER contributions using a generalized logistic and exponential function, respectively. Shown are the effect of scan rate (A), HCl concentration (B), and rotation rate (C).

Figure 4.7 shows the pre-peak current determined after applying the two-step baseline to correct for the superimposed BER and CER currents, and its response to various experimental parameters. No effect from rotation rate is apparent, suggesting that the rate-limiting step is surface-confined. The peak also shows complex dependencies on scan rate and chloride concentration, as shown in Figure 4.8.

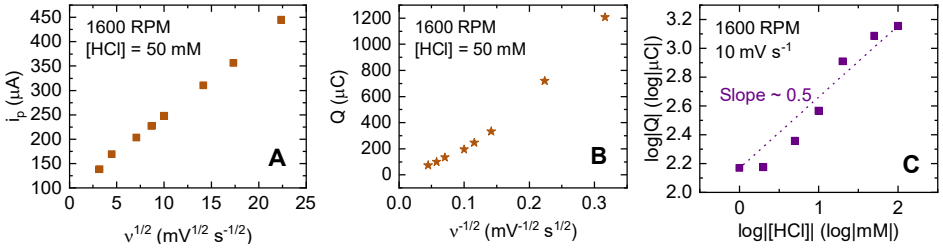

Figure 4.8: Scan rate and $[Cl^-]$ relationships as determined for the CER pre-peak, using data from Figure 4.7. Shown are the dependency of the peak current vs. the square root of the scan rate (A), dependency of the peak charge on the inverse square root of the scan rate (B), and a log-log plot of the peak charge versus chloride concentration (C).

In case of a surface-confined reaction, one would expect a linear dependence between peak current and scan rate, but this is not observed in Figure 4.8. The pre-peak has a linear dependence of the peak current on the *square root* of the scan rate, an approximately linear dependence of peak charge with the inverse square root of the scan rate, and a 'surface charge order' of about 0.5 (i.e. a square root relationship between peak charge and chloride concentration). Especially the linear dependency of peak current vs. square root scan rate is striking. This outcome is usually expected for a solution species reacting at a stationary electrode, where the square root relationship arises from the dependence of the diffusion layer thickness on time. It should not apply under hydrodynamic conditions, where the thickness is constant in time. A possible explanation for this, as well as the general behavior of the pre-peak, is that surface diffusion is involved. Formation of BrCl is expected to proceed via an electrochemical Langmuir-Hinshelwood mechanism, such as during CO stripping from Pt,[222] which requires concerted steps of two different reaction surface species instead of one. We found that the pre-peak is effectively irreversible and does not re-appear in the backward scan, even when using a lower potential of scan reversal (Figure A 9.4.24). This implies that it requires a precursor that is only formed during the forward scan (Figure A 9.4.25).

4.3.7. UV-Vis studies of parallel oxidation of bromide and chloride

In the RRDE experiments, we ascribed the three main oxidation events to the formation of Br_2, BrCl and Cl_2 based on a kinetic analysis. It is highly desirable to corroborate these results with a method capable of ascertaining the identity of the products formed. UV-Vis spectroscopy allows this, since all species in Table A 9.4.1 (except Br^- and Cl^-) have a secondary adsorption band (or shoulder, in case of Br_3^-) that falls in the range 325 – 390 nm, which is accessible when measuring a transparent electrode on a glass substrate. We applied a stepwise potential vs. time program constituting 25 mV steps with a 30 s duration, between 1.060 – 1.485 V vs. NHE (Figure A 9.4.26A), in order to study both the effect of increasing potential, as well as shifts in solution composition during progressing oxidation reactions for each constant potential. Changes in the total transmission were measured after passing the beam through the back of the Pt/FTO electrodes and through the electrolyte, to probe the Pt interface as well as halogen species in the surface layer.

The spectra in Figure 4.9 show the effect of increasing bromide concentration and were taken at potentials related to regions of interest, as seen in the corresponding currents in D. The BER

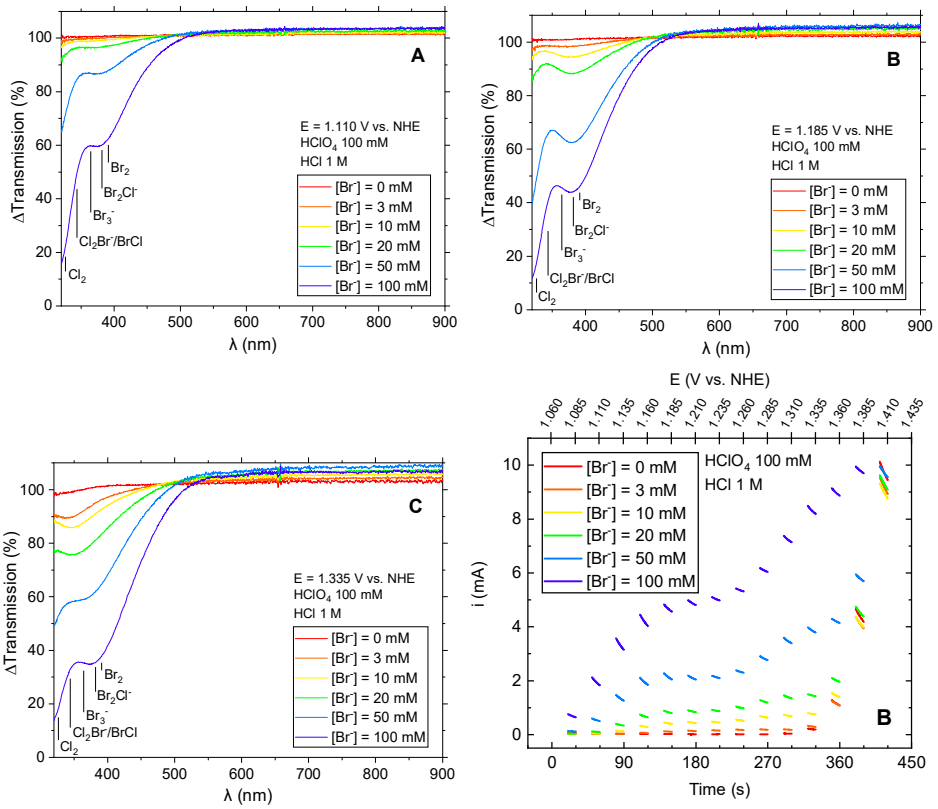

Figure 4.9: UV-Vis measurements of a stationary Pt/FTO electrode in a solution of 0.1 M $HClO_4$ + 1 M HCl, in presence of various [HBr]. A, B and C: UV-Vis spectra measured as function of bromide concentration, after stepping the potential up to 1.110 V (A), 1.185 V (B) and 1.335 V (C), in 25 mV steps of 30 s each. Spectra are shown of 10 seconds after applying the relevant potential. Previously published[210] wavelengths of peak adsorption are indicated for each relevant species. D: Corresponding currents measured during the experiments. Only the final 10 seconds of each potential step are shown for clarity (see Figure A 9.4.26B for full data). Upper axis shows the potentials applied at each moment in time.

has significant activity at 1.110 V (A) and reaches a plateau around 1.185 V (B). The CER becomes just possible at 1.335 V (C), based on the comparison with bromide-free experiments (red trace in D). Features seen in the spectra are always the sum of a mixture of species (section 4.3.2). In Figure 4.9A, Br_3^- contributes the most strongly to the signal due to its high extinction coefficient.[210] Once the potential increases to 1.185 V (Figure 4.9B), the dominant species is Br_2Cl^-. This can be explained by depletion of Br^- near the surface, which shifts the local equilibrium from Br_3^- to Br_2 and subsequent reaction with Cl^-. This is supported by a strong correlation between the peak height relative to its shoulder at 383 nm and the extent to which the BER approaches the current plateau (Figure A 9.4.27). Increasing the potential further to 1.335 V, where the CER can occur, leads to a substantial decrease in transmission in the region 320 – 360 nm. This is clearly related to the formation of Cl_2, $BrCl_2^-$ and BrCl in solution, which all adsorb in this wavelength window.

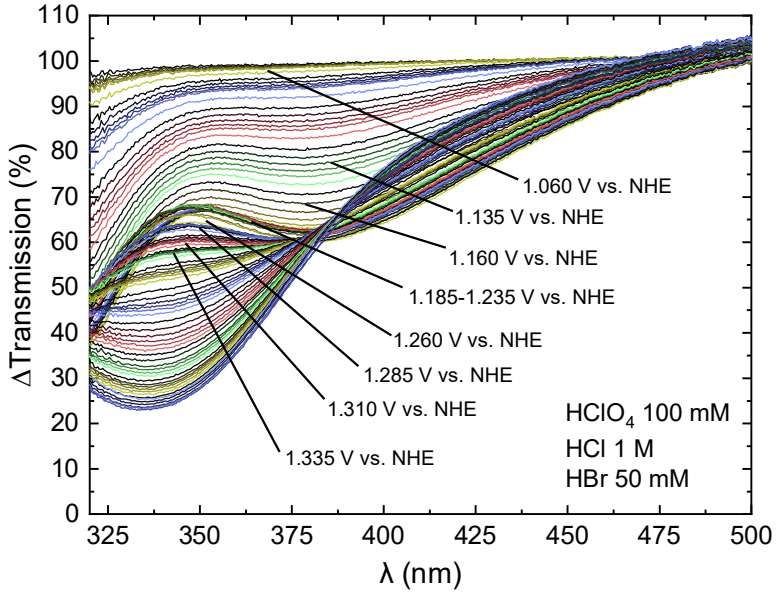

Figure 4.10: Complete set of UV-Vis experiments for parallel bromide and chloride oxidation in 1 M HCl and 50 mM HBr, zoomed on the region where the halogen species adsorb. Colors denote different potential steps, some values of which are indicated. Color gradients from dark to light indicate time evolution of the spectra during each potential step.

When examining the currents recorded in parallel with UV-Vis in Figure 4.9D, we once more observe a pre-wave that precedes the CER onset (onset 1.260 V), and becomes more prevalent as the bromide concentration increases. This pre-wave corresponds quite well to results from the RRDE experiments, and suggests that BrCl is formed electrochemically. Further evidence for its formation comes from Figure 4.10, where we regard the complete time evolution of a typical UV-Vis experiment during parallel bromide and chloride oxidation. Between 1.110 V and 1.260 V, the spectra show the previously described peak of Br_2Cl^- near 380 nm. As the potential is stepped beyond 1.260 V, the transmission in the region 340 – 360 nm disproportionally lowers, which can only be caused by the formation of Cl_2, BrCl or $BrCl_2^-$. We note that in bromide-free conditions, Cl_2 becomes only just detectable around 1.350 V, and dominates at 1.400 V (Figure A 9.4.28). The change at 1.260 V therefore implies the formation of BrCl or $BrCl_2^-$ without the presence of Cl_2 in solution, such that they must have been formed directly by BrCl formation on the electrode. Similar results were obtained under conditions of higher bromide concentrations (Figure A 9.4.29), as well as lower overall halide concentrations (Figure A 9.4.30 and Figure A 9.4.31). The UV-Vis spectra thus confirm the observation in the RRDE experiments of an intermediate oxidation reaction occurring between the BER and CER.

In Figure 4.9, we note an increase in transmission in the wide region of 550 – 900 nm for experiments involving high bromide concentrations combined with high potentials. This increase was likely caused by transient Pt dissolution during vigorous halogen oxidation. The used Pt samples had a low thickness of roughly 5 nm, to limit scattering of the beam. Therefore any dissolution had a relatively large effect on the transmission.

4.4. Discussion and conclusions

The study of parallel Br^- and Cl^- oxidation on Pt revealed significant differences in their interaction. Bromine evolution exhibited linear Tafel slopes of 25-35 mV/dec and a Br^- reaction order $\mathcal{R}_{Br^-}$ that is probably close to 2 at low overpotentials. In the presence of chloride, the reaction becomes increasingly kinetically controlled, and Tafel curves have steeper slopes and becomes less linear. The BER chloride reaction order $\mathcal{R}_{Cl^-}$ progressed from roughly 0 to -1 as the chloride concentration $[Cl^-]$ increases. All these phenomena could be quite well modelled by the Tafel recombination-controlled mechanism, describing the competitive adsorption of Br^- and Cl^- with a simple Langmuir isotherm in the Volmer pre-equilibrium. The results suggest that the effect of Cl^- on the BER is 'simple' competitive adsorption through site blocking. The competing effect of Cl adsorption will likely become more prevalent at higher $[Cl^-]/[Br^-]$ ratios, such as in seawater.

Contrary to the BER, the Langmuirian Volmer-Tafel approach fails for accurately modelling the CER kinetics and the competing effect of bromide, as neither the CER itself (in absence of Br^-) nor the CER during parallel Br^- and Cl^- oxidation are properly described by this model. In absence of Br^-, the CER displays linear Tafel regions between 35-45 mV/dec, and $\mathcal{R}_{Cl^-}$ values that are consistently close to 1, irrespective of $[Cl^-]$ or overpotential η. The addition of Br^- again leads to linear Tafel regions but with significantly higher values of ~100 mV/dec, and $\mathcal{R}_{Cl^-}$ varies between 0 and 2 as function of Cl^-. The parallel formation of a platinum oxide layer at CER-relevant potentials and its effect on the apparent oxidation kinetics remains an incompletely understood issue, but it should not be the origin of the Br^--induced drastic change in the CER kinetics. The suppressing effect of 10 mM Br^- leads to a decrease of the PtO_x charges during CER experiments of 10-30% (Figure A 9.4.19 and Figure A 9.4.20), but the oxide growth behavior was very similar to Br^--free conditions. It thus seems reasonable that the interaction of the PtO_x layer with the occurring CER, although not exactly understood due to its complexity, is not changed significantly by bromide. The change in CER kinetics should originate from a direct effect of Br^- on the adsorption and recombination of chloride.

In addition to the BER and CER, the formation of the interhalogen BrCl likely takes place during parallel Br^- and Cl^- oxidation on Pt. Evidence for this comes from an oxidation 'pre-peak' that thermodynamically precedes the CER, and UV-VIS experiments that indicate that an 'intermediate' oxidizing species is formed at potentials lower than the CER onset. RRDE experiments suggested that BrCl evolution takes place via an irreversible surface reaction with a dependence on scan rate that suggests that surface diffusion plays a role. The process was strongly dependent on the preceding electrode treatment and probably depends on a specific intermediate.

This study has shown that 2-electron halogen oxidation reactions may still be more complicated than previously thought. While the BER conformed surprisingly well to a simple Langmuir pre-equilibrium model, previous studies on poly- and monocrystalline Pt surfaces show that the surface should be virtually saturated with Br^* near the onset of the BER.[223–225] A similar argument holds for Cl^* and the CER.[226–228] The value of θ should thus be essentially constant versus potential when the respective halogen evolution conditions proceed, and the reaction rate should be virtually independent of E or $[X^-]$ in case of the V-T mechanism. The

reactions nonetheless behave as if θ is still low near the onset, which suggests that the pre-adsorbed species are not the actual reactants. This situation is very similar to the evolution of H_2 on Pt, which takes place while Pt is demonstrably saturated by H^*, yet shows Tafel slopes of ~ 30 mV/dec at low overpotentials. To explain this disparity, the concept of 'overpotential-deposited hydrogen'[229] has been invoked. A similar approach might be advisable for the BER and the CER. The apparent differences between the reactions is then perhaps due to differing interactions of overpotential-deposited Br^* and Cl^* with the emerging PtO_x layer. To better describe the CER, an approach that also includes a description of local interactions between adsorbed species may be needed, as has been done previously for competitive adsorption of Br^- and H^+ on Pt(100).[230] The use of a more complex isotherm (such as Frumkin) will probably not be more accurate as long as it still relies on the mean-field approximation, which cannot account for structured adlayers. In this regard, additional studies of halogen evolution on single crystal Pt surfaces would be very insightful.